Tidal stream turbine control: An active disturbance rejection control approach

Zhibin Zhou, Seifeddine Ben Elghali, Mohamed Benbouzid, Yassine Amirat, Elhoussin Elbouchikhi, Gilles Feld

Z. Zhou, S. Benelghali, M. Benbouzid, Y. Amirat, E. Elbouchikhi, G. Feld, "Tidal stream turbine control: An active disturbance rejection control approach," Ocean Engineering, vol.202, 107190, pp. 1-9, march 2020

Tidal Stream Turbine Control: An Active Disturbance Rejection Control Approach

Zhibin Zhou[1], Seifeddine Ben Elghali[2], Mohamed Benbouzid[3,4], Yassine Amirat[1], Elhoussin Elbouchikhi[1], and Gilles Feld[1]

[1]*ISEN Yncréa Ouest, UMR CNRS 6027 IRDL, Brest, France*

[2]*Aix-Marseille University, UMR CNRS 7020 LIS, Marseille, France*

[3]*University of Brest, UMR CNRS 6027 IRDL, 29238 Brest, France*

[4]*Shanghai Maritime University, 201306 Shanghai, China*

zhibin.zhou@isen-ouest.yncrea.fr, seifeddine.benelghali@lis-lab.fr, Mohamed.Benbouzid@univ-brest.fr, yassine.amirat@isen-ouest.yncrea.fr, elhoussin.elbouchikhi@isen-ouest.yncrea.fr, gilles.feld@isen-ouest.yncrea.fr

Abstract— As an emerging technology to harness the marine current energy, tidal stream turbine (TST) systems have been developed due to high predictability and energy density in tidal current resources. However, considering that various challenges such as swell disturbances, unknown disturbances, or parameter uncertainties may deteriorate the system performance, it is interesting to investigate alternative control strategies to the conventional proportional-integral (PI) controls. In this paper, the active disturbance rejection control (ADRC) approach is proposed to replace PI controllers in the conventional generator-side control scheme. In this approach, two ADRC schemes (cascaded and second-order ADRC strategies) are respectively applied and compared to achieve MPPT under current velocity and turbine torque disturbances. Performances of the proposed ADRC approaches are compared to PI and sliding mode control strategies. Energy production during swell wave disturbance is also evaluated under these control strategies. The comparisons show that the cascaded ADRC has better performance than the second-order approach. Moreover, the cascaded ADRC is tested under parameter variations to evaluate its robustness. The carried out simulation-based comparative study shows the effectiveness and advantages of the cascaded ADRC strategy over conventional PI controller in terms of fast convergence, overshoots elimination, and improved robustness under disturbances and parameter uncertainties.

Keywords— Tidal stream turbine, disturbance rejection control, maximum power point tracking, robustness.

I. INTRODUCTION

Tidal stream turbine (TST) generation systems, based on similar principles of wind power systems, have been developed to generate electricity from tidal-driven currents during the last decades. Advantages of TST generation systems are related to the high predictability (in hourly time scale) and high energy density of the tidal-driven currents [1-2]. Although challenges such as submarine installation and maintenance do exit, TST generation systems are still considered to be a promising power supplying solution for some remote islands or coastal areas. In fact, various demonstrative TST projects have been successfully industrialized and they are entering the pre-commercial stage [3-4]. For achieving compact structure and reducing maintenance requirements, several TST projects adopt turbines with nonpitchable blades and choose permanent magnet synchronous machine as generator [5].

The power harnessed by a TST is generally proportional to the cubic marine current velocity and the turbine power coefficient. For a turbine with fixed-pitch blades, the turbine power coefficient (C_p) depends on the tip speed ratio (TSR), which can be controlled by the generator rotational speed. Therefore, speed control in TST generation system can be necessary in order to capture maximum power under the varying marine current speed. A previous study in [6] shows that under strong swell wave disturbances, a speed control with filter-based reference or a torque-based control can achieve smoother produced power.

However, in that work only classical proportional-integral (PI) controllers are used and other kind of disturbances such as sudden current flow velocity change and unpredictable turbine mechanical torque changes are not considered.

Although PID control is the most popular control strategy in industrial applications due to its simple structure and relative easy parameter tuning, it may suffer several drawbacks such as: 1) the controller implementation is often done without the derivative part (D) due to noise sensitivity; 2) slow response or overshoot caused by the integration action; 3) controller parameter tuning usually requires accurate plant model and parameters, which may be unavailable or present uncertainties under different operation conditions. To improve the transient performance of PID controllers, system identification and intelligent techniques are introduced [7]. Fuzzy PID controllers can have better performances with adaptive controller gains, however the design of membership function and rule sets could be difficult and complex [8-9]. In modern control, there are several advanced control strategies, which are interesting. The model predictive control (MPC) and linear quadratic regulator (LQR) require analysis of the space-state model of the plant. They have good performance around the steady-state operating point but are not robust and could be sensitive to unmodeled dynamics and external disturbances [10-11]. As a group of variable structure controllers, higher-order sliding (HOSM) controllers are considered as a powerful control tool for nonlinear systems under parameter uncertainties. HOSM is developed to reduce chattering, which is caused by unmodeled dynamics that increase the relative degree of the plant [12]. In various HOSM control laws, high-order time derivatives of the sliding variable are often required. However, measuring high order derivatives in practice is often with high noises and not feasible. In this case, high-order finite-time convergent observer based on the symbolic function should be used [13]. The choice of the control laws and parameter tuning of the HOSM could be difficult when the boundary conditions of the variation range or variation rate of certain system parameters are unavailable.

In [14-16], a relatively new design structure for controllers, namely active disturbance rejection control (ADRC), was proposed. ADRC is not based on plant model analysis, because system behaviors could change unexpectedly in practice under disturbances and the plant models may therefore become unreliable. As an emerging approach, ADRC uses a controller-observer pair to treat external and internal disturbances, plant parameter variations or uncertainties as an element not to be modeled analytically but to be rejected as a generalized “total disturbance”; in this way the control signal responds directly to cancel the “total disturbance” and thus making the controller design almost model-free [17]. Linear ADRC (LADRC) enables to apply parameter-tuning methods based on close-loop bandwidth and observer bandwidth according to desired frequency or time domain performances [18-19]. However, the study in [20] shows that the limitation of sensor bandwidth could degrade the closed-loop performance of the LARDC. Various parameter uncertainties and external disturbances exist in PM machines, a comprehensive overview on disturbance and uncertainty estimation and attenuation (DUEA) techniques including ADRC is given in [21]; it shows that DUEA has a better balance among performances compared to other robust control and adaption control methods. In [22-23], ARDC are applied to the speed controller of PM machines, however PI controllers are still used in the current loops. In a recent work [24], ADRC was applied on a laboratory-scaled small PM machine and compared to PI and SM controls. Although the comparison carried out in [24] is of some interest, there were several issues such as the size of the used PM machine that does not fit tidal stream turbine systems power level for deployment, ADRC was only applied in the speed control loop, and the robustness issue has not been addressed while it is a critical issue in a marine context (i.e. parameter variations). All these issues will be addressed in this work while a control alternative, namely a second-order ADRC approach, will be developed and compared to the proposed cascaded ADRC approach.

Figure 1 shows a classical double-loop control scheme of a permanent magnet synchronous generator (PMSG); the current loop control is usually based on PI controllers; and the speed controller can be either PI controller or other advanced controller. In order to fully benefit from the ADRC strategies advantages, an all-ADRC approach, as shown in Fig. 2, is proposed in this work. In this approach, all the controllers both in speed and current loops are designed by ADRC strategies. In the proposed cascaded ADRC approach, the decoupling terms in the classical PI current control loops are not needed and thus the dependence of system parameters can be reduced. Using a higher order ADRC controller to combine the speed ADRC controller and the *q*-axis ADRC current controller can achieve a possible variant of this ADRC approach.

Nonlinear ARDC controllers are applied in this work to fully maintain the advantages of "large error, small gain; small error, large gain" compared to LADRC. The proposed all-ADRC approach is applied to a 500 kW TST generation system to achieve the MPPT task under different kinds of disturbances and parameter variations.

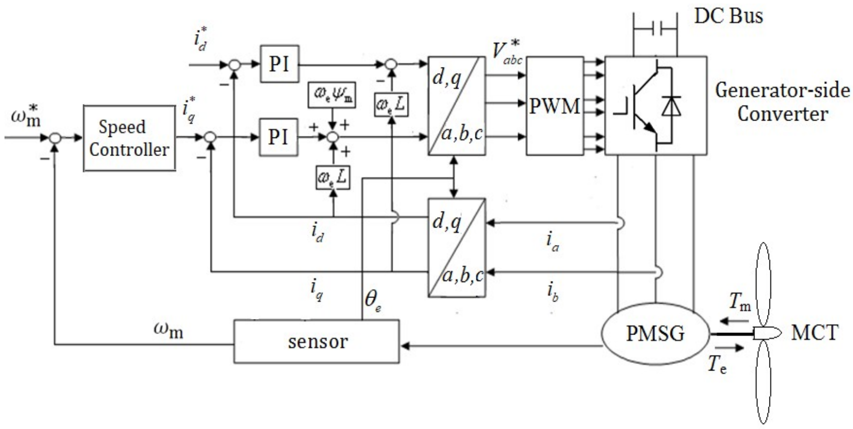

Fig. 1. Classical control scheme for a PMSG-based TST system.

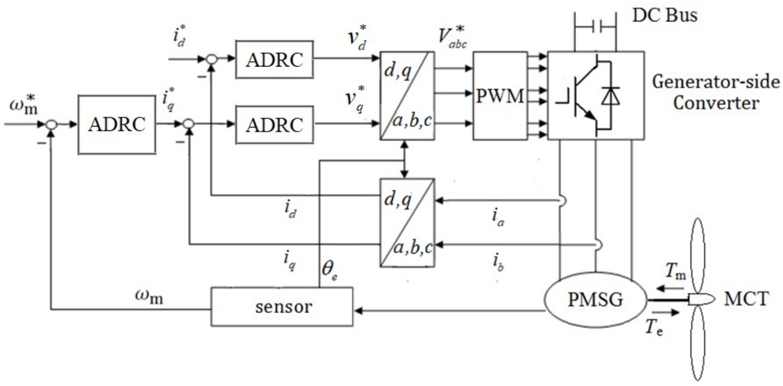

Fig. 2. Proposed ADRC control scheme for a PMSG-based TST system.

In Section II, the PMSG-based TST system model and classical controller design for the TST generation system are presented. Then, the proposed ADRC approach and the controller design are presented in Section III. In Section IV, simulation results of different control strategies under tidal current speed and turbine torque disturbances are compared. Energy production performance under swell effect is also presented. In Section V, parameter uncertainties are applied to verify the proposed ADRC robustness. Section VI gives the conclusion.

II. CLASSICAL CONTROL FOR A TST SYSTEM

The mechanical power extracted by a TST can be calculated by the following equation.

$$P = \frac{1}{2}\rho C_p(\lambda)\pi R^2 V_{tide}^3 \tag{1}$$

In (1), the seawater density ρ and the turbine radius R are constants; V_{tide} is the velocity of marine tidal current; C_p is the turbine power coefficient. For a given turbine, the C_p curve may be approximated as a function of the pitch angle and the tip speed ratio λ. The considered TST is a fixed-pitch blade one, therefore C_p depends only on λ. For typical MCT prototypes, the optimal C_p value is estimated to be in the range of 0.39-0.45 [3]. Figure 3 shows the C_p curve used in this work. The maximum C_p value is 0.41, which corresponds to a tip speed ratio of 6.3. This value is considered as the optimal tip speed ratio (λ_{opt} = 6.3) for obtaining the maximal C_p value under varying tidal current condition.

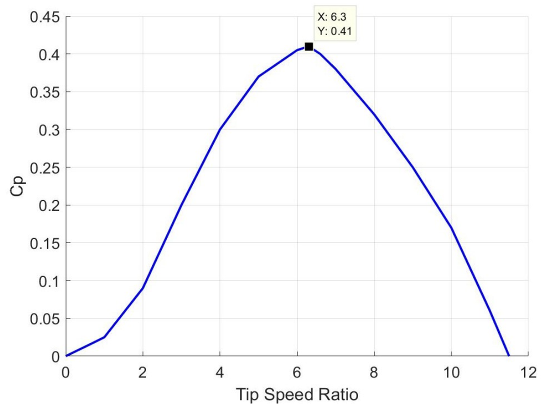

Fig. 3. C_p curve of the studied TST.

A basic MPPT control can be realized by controlling the generator speed to regulate the turbine rotational speed according to tidal current velocity. The speed reference for the generator can be given by (2) for the considered direct-driven TST:

$$\omega_m^* = \frac{\lambda_{opt} V_{tide}}{R} \tag{2}$$

For the PMSG, the d-q frame model is described by (3).

$$\begin{cases} v_d = R_s i_d + L_d \dfrac{\mathrm{d}i_d}{\mathrm{dt}} - \omega_e L_q i_q \\ v_q = R_s i_q + L_q \dfrac{\mathrm{d}i_q}{\mathrm{dt}} + \omega_e L_d i_d + \omega_e \psi_m \\ T_e = \dfrac{3}{2} n_p \left[\psi_m i_q + (L_d - L_q) i_d i_q \right] \\ J \dfrac{\mathrm{d}\omega_m}{\mathrm{dt}} = T_m - T_e - f_B \omega_m \end{cases} \tag{3}$$

In (3), v_d, v_q and i_d, i_q are stator voltages and currents in the d-q axis respectively; R_s is the stator resistance; L_d, L_q are inductances in the d-q axis ($L_d = L_q = L_s$ for a non-salient machine is considered in this work); ω_e, ω_m are machine electrical and mechanical speed; T_e , T_m are respectively the machine electromagnetic and the mechanical torques; n_p is the generator pole pair number; ψ_m is the flux linkage created by the rotor permanent magnets; J is the total system inertia and f_B is the friction coefficient associated to the mechanical drivetrain. A 500kW TST system is considered in this work and the system parameters are given in the Appendix.

In the classical control scheme shown in Fig. 1, the current loop response is much faster than the speed response and the current controller tuning is usually easier than the speed controller. Therefore, PI control are applied for the two current loops in this section, and then two different control strategies – PI and sliding mode (SM) control will be applied to the speed controller. The controllers should be well tuned to serve as a sound base for later comparison with the proposed ADRC strategies.

A. Proportional-Integral Control

The tuning of the two PI controllers (shown in Fig. 1) in the current loops is to be presented firstly. Same parameters can be used for both PI current controllers due to the similar dynamics for i_d and i_q loops. The open-loop transfer function of the PI control based current loop can be expressed as:

$$G_0(s) = \frac{K_{pc}(\tau_{ic}s+1)}{\tau_{ic}s} \cdot \frac{1/R_s}{\left[(L_s/R_s)s+1\right]\left(T_{\Sigma I}s+1\right)} \tag{4}$$

with K_{pc} and $K_{ic} = 1/\tau_{ic}$ as the current-loop controller gains and $T_{\Sigma I}$ (which is much smaller than the electrical time constant L_s/R_s) as a small time constant standing for current sensor and power converter delays. Based on the dominant pole cancelation method and with a desired damping factor (0.707 in this work) for the close-loop transfer function, the following controller gains can be chosen for the current-loop PI controllers:

$$\begin{cases} K_{ic} = R_s / L_s \\ K_{pc} = R_s / \left(2T_{\Sigma I}K_{ic}\right) \end{cases} \tag{5}$$

The speed controller will generate the q-axis current reference i_q^*. The d-axis current reference i_d^* can be set to 0 for maximizing the electromagnetic torque for a given stator current. The PI speed controller parameters can be tuned by many ways, and in this work the non-symmetrical optimum method (NSOM) is chosen. As one analytical method, the NSOM relies on a second-order approximated model of the plant with a generalized time constant ($T_Q = 1/\omega_Q$), which includes all the time delays in the speed loop, and K_Q, which represents the slope rate of open-loop step response. These two parameters can be deduced from a series of step response tests in simulation or in practice. By the NSOM, the parameters of the PI speed controller can be obtained from [25] as follows:

$$\begin{cases} K_{ps} = \gamma_c \dfrac{\omega_Q}{K_Q\sqrt{\alpha_c}} \\ K_{is} = \dfrac{\omega_Q}{\alpha_c} \end{cases} \tag{6}$$

In (6), the correcting gain fact γ_c is defined in terms of the desired resonant peak value M_c; the parameter α_c is calculated by a phase advance $\Delta\varphi$, which depends on γ_c. More details of the NSOM tuning procedure can be found in [26].

B. Sliding Mode Speed Control

To improve the PMSG speed control performance, HOSM can be applied [27-29]. In this work, the super-twisting sliding mode control strategy is applied to the speed controller as an alternative to the PI one. The sliding variable is defined as the speed tracking error,

$$s_1 = e = \omega_m^* - \omega_m \tag{7}$$

and the controller output is calculated by

$$u = i_q^* = K_1 \cdot |s_1|^{0.5} \operatorname{sign}(s_1) + K_2 \int \operatorname{sign}(s_1) \tag{8}$$

The lower limits of the gains K_1 and K_2 for the super-twisting control law can be calculated with bounding information of certain parameters variation range and variation rate [30]. Generally, higher gains are needed to cover higher parameter uncertainty and larger disturbances. In this work, K_1 = 1200 and K_2 = 500 are chosen for the studied TST system.

III. ADRC ALTERNATIVE APPROACH FOR THE TST SYSTEM

A. Active Disturbance Rejection Control

From the previous PI speed controller tuning procedure, it can be noted that the PI gains relay on the knowledge of plant parameters or require some tests to obtain an approximate plant model. However, disturbances or nonlinear dynamics are not considered in PI controller designs.

To overcome these drawbacks, ADRC uses a nonlinear controller (NLC) with an extended state observer (ESO) to obtain fast convergence and effective disturbance rejection. A stand formulation for applying ADRC is based on a canonical state-space expression of the plant with the "total disturbance" as an extended state variable. The ADRC controller order depends on the derivative order of the target variable to be controlled [24]. The first-order derivation of the plant output y can be formulated by

$$\begin{cases} \dot{x}_1 = F + b \cdot u \\ y = x_1 \end{cases} \tag{9}$$

In (9), u is the plant input, b is a constant, and F represents the total disturbance (which combines all the known dynamics and unknown disturbances). Then, F is treated as an extended state variable x_2 to be estimated by the ESO. The first-order ADRC controller diagram is illustrated by Fig. 4. In this figure, e is the tracking error; b_0 is a roughly estimated value of the constant b of the plant described in (9); and the ESO has two outputs: z_1 is an estimation of the plant output y; and z_2 is the estimated total disturbance F.

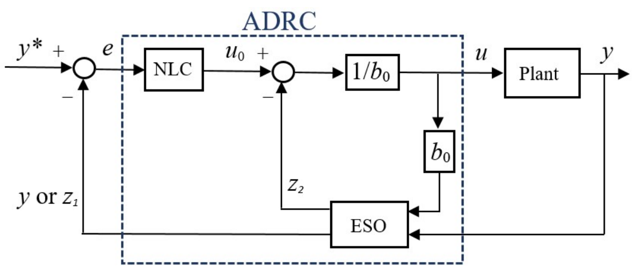

Fig. 4. General first-order ADRC control diagram.

The nonlinear function called *fal* is applied in the ADRC,

$$fal(x,\alpha,\delta) = \begin{cases} |x|^{\alpha}\,\mathrm{sign}(x), & |x| > \delta \\ \dfrac{x}{\delta^{1-\alpha}}, & |x| < \delta \end{cases} \tag{10}$$

with x as the main input representing some kind of error information; $0 < \alpha < 1$ enables the function value to have a reducing effect with large x input and $\delta > 0$ introduces a linear zone to avoid too big function value for small x around 0.

The ESO of the ADRC can then be constructed as

$$\begin{cases} \varepsilon = z_1 - y \\ \dot{z}_1 = z_2 + b_0 u - \beta_1 \cdot fal(\varepsilon,\alpha_1,\delta) \\ \dot{z}_2 = -\beta_2 \cdot fal(\varepsilon,\alpha_2,\delta) \end{cases} \tag{11}$$

with β_1, β_2 as the ESO gains. The NLC is given as $u_0 = k_1 fal(e,\alpha_0,\delta)$, with k_1 as the controller gain. The ADRC controller output is $u = (u_0 - z_2)/b_0$. It is also possible to move the block $1/b_0$ on the z_2 signal channel in Fig. 4 and thus making the controller output $u = u_0 - z_2/b_0$. This could be helpful to reduce the NLC output u_0 and its controller gain k_1, when the constant b_0 is very large.

B. Cascaded ADRC Control

In the proposed cascaded ADRC control for the tidal stream turbine generation system (Fig. 2), the current loop ADRC controllers are constructed based on the first-order derivation of the d-q axis currents.

$$\begin{cases} \dot{i}_d = \dfrac{1}{L_d}\left(-R_s i_d + \omega_e L_q i_q\right) + \dfrac{1}{L_d} v_d^* \\ \dot{i}_q = \dfrac{1}{L_q}\left(-R_s i_q - \omega_e L_d i_d - \omega_e \psi_\mathrm{m}\right) + \dfrac{1}{L_q} v_q^* \end{cases} \tag{12}$$

When comparing (12) with the standard formula (9), it can be seen that for the surface-mounted PMSG ($L_d = L_q = L_s$), the constant $b = 1/L_s$ is the same for the dynamic model of d-q axis currents. Although the total disturbance F has different expressions in d-q current loops, the same ADRC current controller can be used for both current loops for the reason that the total disturbance F does not need to be known or modeled, but it can be estimated by the ESO. In this case, only the basic knowledge of $b_0 = 1/L_s$ is required for the ADRC current controller. Applying the ADRC approach, the q-axis current controller is designed as (13); and the d-axis current controller can be constructed in the same way.

$$\begin{cases} \varepsilon = z_1 - i_q \\ \dot{z}_1 = z_2 + (1/L_s)\cdot u - \beta_{1c}\cdot fal\left(\varepsilon, 0.5, 2\right) \\ \dot{z}_2 = -\beta_{2c}\cdot fal\left(\varepsilon, 0.25, 2\right) \\ e = i_q^* - z_1 \\ u_0 = k_{1c}\cdot fal\left(e, 0.5, 2\right) \\ u = u_0 - L_s z_2 = v_q^* \end{cases} \tag{13}$$

In (13), the first three equations are the ESO in the ADRC current controller to estimate the current by z_1 and the total disturbance of the concerned current loop by z_2. The last three equations describe the NLC and the output of the ADRC current controller. The ESO and NLC gains of the ADRC current controller are tuned intuitively by trial and error as $\beta_{1c} = 90000$, $\beta_{2c} = 60000$, $k_{1c} = 150$.

For the speed controller, the variable to be controlled is the generator rotor speed $y = \omega_m$, and the controller output is the q-axis current reference $u = i_q^*$. Based on the first-order derivative of the rotor speed,

$$\dot{\omega}_m = \left(-\frac{T_m}{J} - \frac{f_B \omega_m}{J}\right) + \frac{1.5 n_p \psi_\mathrm{m}}{J} i_q^* \tag{14}$$

the ADRC speed controller can be designed as follows.

$$\begin{cases} \varepsilon_s = z_1 - \omega_m \\ \dot{z}_1 = z_2 + b_{0s} \cdot u - \beta_{1s} \cdot fal\left(\varepsilon_s, 0.5, 0.01\right) \\ \dot{z}_2 = -\beta_{2s} \cdot fal\left(\varepsilon_s, 0.25, 0.01\right) \\ e_s = \omega_m^* - \omega_m \\ u_0 = k_{1s} \cdot fal\left(e_s, 0.3, 0.01\right) \\ u = \left(u_0 - z_2\right) / b_{0s} = i_q^* \end{cases} \tag{15}$$

In (15), The constant b_{0s} is set close to or equal to the constant $b = 1.5 n_p \psi_m / J$ as found in (14). It should be noted that the ADRC speed controller does not need accurate plant model, which means that the unknown disturbances or variations of the mechanical torque, friction coefficient, rotational speed, and the system inertia can be generalized as the total disturbance and estimated inside the ESO of the ADRC. Due to the fact that the dynamics of the speed loop is much slower than the current loop and considering a quite important system inertia for the studied 500 kW PMSG-based TST system ($J = 4.359 \times 10^4\ \text{kg} \cdot \text{m}^2$), the ESO gains β_{1s}, β_{2s} should be much smaller than those of the current controller. The ESO and NLC gains of the ADRC speed controller are tuned by simulation as $\beta_{1s} = 36$, $\beta_{2s} = 3$, $k_{1s} = 20$.

C. Second-Order ADRC Control

There exists a possibility to merge the cascaded speed ADRC controller and the *q*-axis ADRC controller into one second-order ADRC speed controller if the second-order derivation of the rotor speed is formulated as

$$\begin{cases} \ddot{\omega}_m = F + \dfrac{k_T}{J L_q} \cdot v_q^* \\ F = -\dfrac{\dot{T}_m}{J} - \dfrac{f_B \dot{\omega}_m}{J} - \dfrac{k_T}{J L_q}\left(R_s i_q + \omega_e L_d i_d + \omega_e \psi_m\right) + d \end{cases} \tag{16}$$

In (16), $k_T = 1.5 n_p \psi_m$ is the PMSG torque constant; F is the total disturbance to be estimated and rejected by the second-order ADRC; d represents unknown disturbances. Based on the basic structure of a second-order ADRC proposed in [15], the second-order speed controller for the PMSG-based TST can be designed as follows,

$$\begin{cases} \varepsilon_s = z_1 - \omega_m \\ \dot{z}_1 = z_2 - \beta_1' \cdot \varepsilon_s \\ \dot{z}_2 = z_3 + b_0' \cdot u - \beta_2' \cdot fal\left(\varepsilon_s, 0.9, 0.01\right) \\ \dot{z}_3 = -\beta_3' \cdot fal\left(\varepsilon_s, 0.9, 0.01\right) \\ e_1 = \omega_m^* - \omega_m, e_2 \approx \dot{e}_1 \\ u_0 = k_1' \cdot fal\left(e_1, 0.5, 0.01\right) + k_2' \cdot fal\left(e_2, 1.1, 0.01\right) \\ u = u_0 - z_3 / b_0' = v_q^* \end{cases} \tag{17}$$

In (17), the constant b'_0 can be set as $k_T / J L_s$; the derivative of the tracking error can be approximately calculated by (18), with τ_1 = 0.001 and τ_2 = 0.0015, to avoid direct differentiation of the tracking error which may contain noises or sharp variations; z_1, z_2, and z_3 are the estimations of the rotor speed, its derivative and the total disturbance, respectively; β'_1, β'_2, and β'_3 are the ESO gains and k'_1 and k'_2 are the NLC gains of the second-order ADRC controller.

$$e_2 = \frac{1}{\tau_2 - \tau_1}\left(\frac{1}{\tau_1 s + 1} - \frac{1}{\tau_2 s + 1}\right) \cdot e_1 \tag{18}$$

Although the second-order ADRC speed controller enables to generate v_q^* directly from speed tracking error, this approach involves a more complicated controller design and large gains have to be used in the ESO because the "total disturbance" needed to be estimated by the second-order ADRC is greatly increased compared to the first-order one.

IV. SIMULATION AND COMPARATIVE STUDY

In this section, a 500kW direct-driven PMSG based TST (system parameters are listed in the Appendix) is studied. The proposed cascaded ADRC approach will be compared with the second-order ADRC approach, the classical PI control approach, and the hybrid speed sliding mode plus PI current control strategy. These four control strategies are shortened as ADRC, ADRC2, PI and SM in the following comparison study.

A. Control Performance Evaluation under Disturbances of Current Velocity and Torque

In this part, the current velocity is considered as a constant value of 2m/s during 15s. A sudden current velocity fall (with -0.7m/s as the peak) is applied during 6 ~ 6.6s, and a large turbine torque thrust of 140kNm (equivalent to the nominal torque of the PMSG) is added at 11~11.5s.

The speed performance of the ADRC approach during the entire 15s will be firstly illustrated and then comparisons with other control methods will be carried out in different time periods. Figure 5 shows that the rotor speed response under the proposed ADRC control strategy converges to the speed reference calculated by MPPT very rapidly. A rate limiter block is added at the reference speed so that step speed changes can be avoided. Therefore, at the starting stage, the speed follows a slop reference. During the tidal current disturbance and the turbine mechanical torque disturbance periods, the tracking error is about 0.03rad/s and 0.01rad/s, which are lower than 1.3% of the steady-state speed of 2.377rad/s.

To compare the ADRC performance with other approaches, smaller time scales should be used. Figure 6 compares the rotor speed response during the startup stage. It can be observed that the PI approach leads to an overshoot of 0.21rad/s, which is 8.8% of the steady-state speed. The SM approach enables reducing the overshoot to 3% (0.08rad/s). ARDC has fastest convergent speed with a negligible overshoot of 0.13%. ARDC2 presents no overshoot while it leads some small steady-state errors and oscillations than the other approaches.

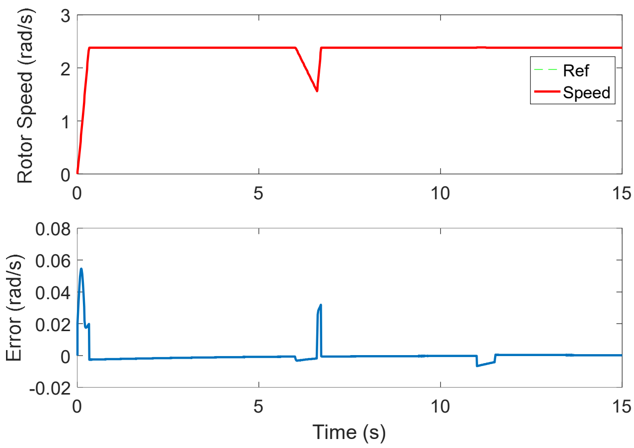

Fig. 5. Generator rotor speed response with ADRC.

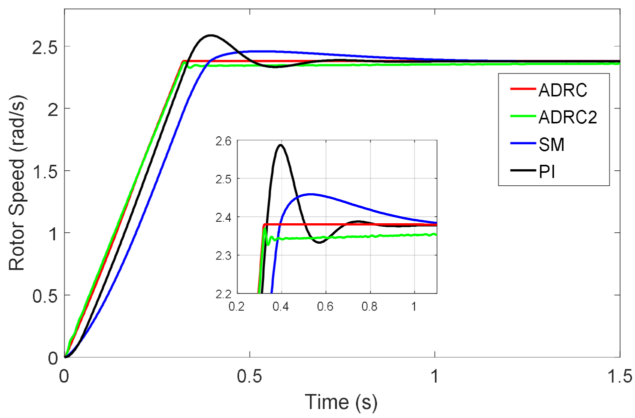

Fig. 6. Speed tracking comparison during starting stage.

Figure 7 shows that, under the current velocity drop disturbance, all the four control approaches are capable to follow a dropping speed reference. However, when the disturbance is cleared at 6.6s, the speed reference has a quick rise to its steady-state value. In this case PI shows the biggest overshoot and longest settle time among other approaches. SM shows a smoother and quicker convergent speed compared with PI; while ADRC and ADRC2 have the fastest convergent speed when the disturbance is cleared. Although the speed performances of ADRC and ADRC2 are very similar, it should be noted that ADRC2 presents small fluctuations, which are caused by torque fluctuations due to the reason that ADRC2 has no q-axis current control loop.

During the torque disturbance, the speed reference is not changed, which means that the ideal rotor speed should keep at the steady-state value of 2.377rad/s. Figure 8 illustrates that the sudden rise of the turbine mechanical torque at 11s leads to a speed rising and the clearance of the disturbance at 11.5s causes a speed dropping for PI and SM; while SM has less fluctuation and a quick performance recovering than the PI approach. Both ADRC and ADRC2 achieve the smallest tracking error and no speed drop error at the clearance of the disturbance at 11.5s. During the torque disturbance, ADRC has a maximum tracking error about -0.007rad/s (as also shown in Fig. 5); ADRC2 seems to have even smaller error compared to ADRC, however speed fluctuations can be seen with ADRC2. Figure 9 shows that ADRC2 leads to bigger torque fluctuations and this explains why speed fluctuations exist in ADRC2. This reveals the drawback of ADRC2 due to the lack of a q-axis current control loop.

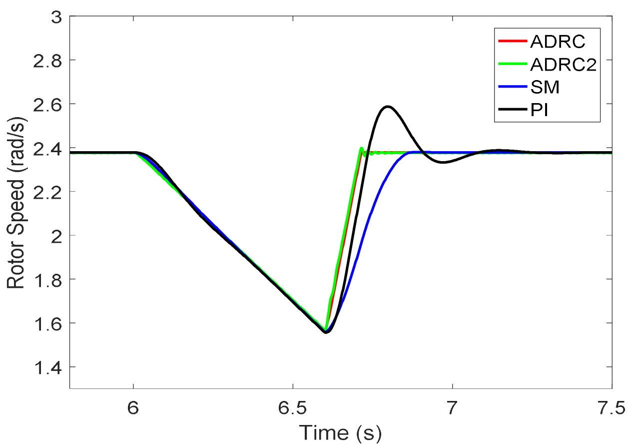

Fig. 7. Speed tracking comparison during current velocity disturbance.

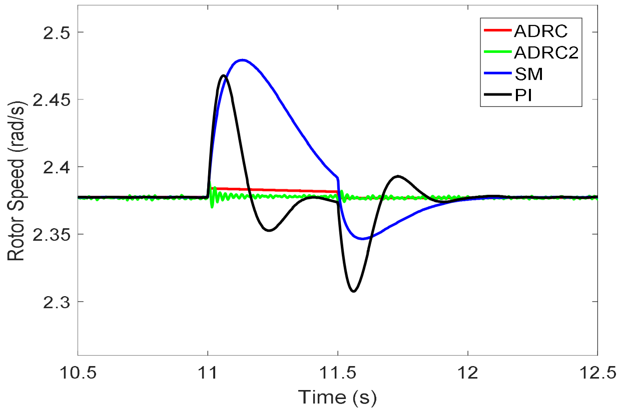

Fig. 8. Speed tracking comparison during turbine torque disturbance.

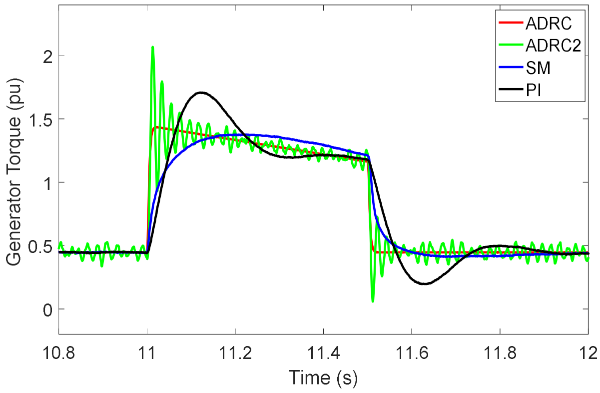

Fig. 9. Generator torque during turbine torque disturbance.

In order to further investigate the control performance (speed tracking) of the above-evaluated strategies, two performance indices ISE (Integral of the Square Error) and ITAE (Integral of the Time-weighted Absolute Error) are evaluated. They are given by [31].

$$ISE = \int_{t_1}^{t_2} e^2(t)dt \tag{19}$$

$$ITAE = \int_{t_1}^{t_2} (t - t_1) \cdot |e(t)| dt \tag{20}$$

In (19) and (20), $e(t)$ is the speed tracking error; t_1 and t_2 represent the time-interval of the studied operating stages. The ISE emphasizes on large overshoot or excessively underdamped behaviors. A small ISE value usually indicates a good capability of large error suppression. The ITAE emphasizes on both initial response error and persistent errors. A low ITAE can therefore reflect a satisfactory general error suppression performance during the duration of interest. ITAE has been also used to tune PID controller parameters [32] or evaluate a controller performance [33]. In our case, both ISE and ITAE are calculated for the three specific operating stages: starting stage (1s ~ 1.5s), current velocity disturbance stage (6s ~ 7.5s,) and torque disturbance stage (11s ~ 12.5s). The achieved performance indices are listed in Table 1.

Based on the calculated performance indices, it has been found that for the starting stage, ADRC has the lowest ISE and ITAE values, which demonstrate that it has a best error suppression capability. SM has a little higher ISE and ITAE values than PI for the reason that a smooth response may lead to a lower error suppression speed in terms of error integration index. This result is coherent with the simulation results shown in Fig. 6. During current velocity disturbance and torque disturbance stages, ADRC2 leads to the smallest ISE and ITAE values and ADRC has very similar results that are much smaller than those of SM and PI. It should be also noted that during the disturbance stages, SM could have smaller ITAE values than PI. This means that nonlinear controllers such ADRC and SM can have generally better disturbance rejection capabilities than constant parameters-PI ones. Although ADRC2 seems slightly better than ADRC according to the index values during the disturbances stages, it should be pointed out that ADRC2 suffers from the lack of a torque loop control (q-axis current loop) and therefore the resulted torque fluctuations are slightly reflected in the speed tracking error due to the system inertia filtering effect. These observations show that ISE and ITAE are interesting indices to evaluate a controller tracking performance. In this context, the speed tracking error suppression capability of the proposed ADRC approach is well validated by these performance indices.

Table 1. Performance indices for three specific operating conditions.

		Starting stage (1s ~ 1.5s)	Current velocity disturbance (6s ~ 7.5s)	Torque disturbance (11s ~ 12.5s)
ADRC	*ISE*	0.00041	0.00009	0.000015
	ITAE	0.00379	0.00296	0.00103
ADRC2	*ISE*	0.00103	0.00002	0.000003
	ITAE	0.0278	0.00281	0.00069
SM	*ISE*	0.0517	0.01536	0.0026
	ITAE	0.0474	0.0378	0.012
PI	*ISE*	0.015	0.00834	0.0011
	ITAE	0.022	0.04	0.0073

B. Control Performance Evaluation under Swell Wave Disturbances

Swell waves are identified as the main cause of short-time power fluctuations in TST generation systems [6]. Figure 10 shows the simulated marine current speed under swell effect (after 4s). Figure 11 illustrates the rotor speed response and its tracking error by the proposed cascaded ADRC approach. It can be observed that the ADRC approach realizes a very good speed tracking under swell-induced disturbances with negligible tracking errors. Figure 12 compares the energy production (calculated by the integration of generator power) under swell disturbance by different control strategies studied in this work. At the end of the simulation (60s), it can be observed that the energy yielding by PI control is about 2736Wh; SM and ADRC2 lead to a slightly better energy yielding with 2737.5Wh and ADRC leads to a best yielding of 2738Wh.

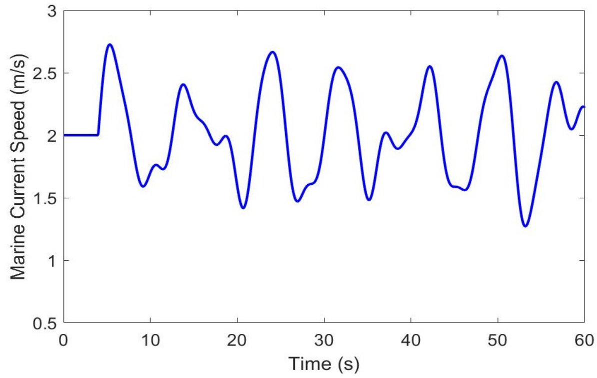

Fig. 10. Marine current speed variations under swell effect.

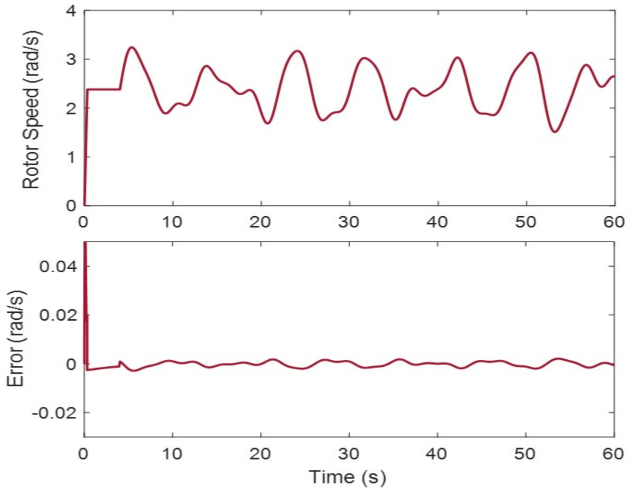

Fig. 11. Generator speed tracking under swell disturbance with ADRC.

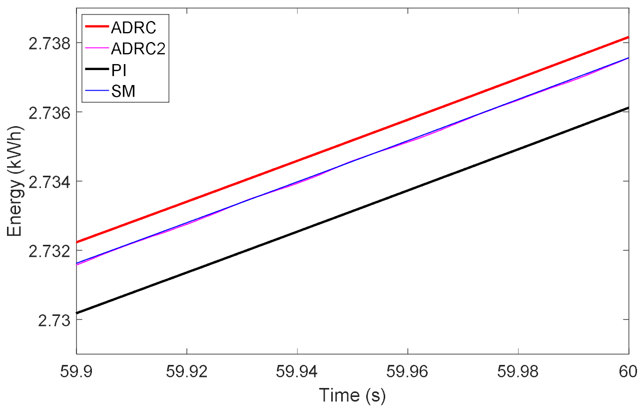

Fig. 12. Comparison of the energy productions.

V. ADRC UNDER SYSTEM PARAMETER VARIATIONS

When the generator resistance R_s and inductance L_s values are changed, the current-loop tracking performances are mainly concerned. Figures 13 and 14 show the tracking errors of *q*-axis current under R_s variations (20% and 500%) and L_s variations (50% and 200%). Large increase of resistance and inductance will cause current pulses, while the performances after 0.5s are quite similar compared to the original parameter case. This illustrates the robustness of the ADRC current controller.

Figure 15 shows the speed responses under different system inertia. Smaller inertia will increase the speed-loop dynamics and make the speed control easier. Larger system inertia requires higher torque to keep the speed rising rate. However, the *q*-axis current, which directly contributes to the torque, is limited by 2 times of nominal current; and this explains the increased tracking error at the starting stage in the 200% inertia case. ADRC works very well to converge the speed to the steady-state value rapidly and results in no speed overshoot.

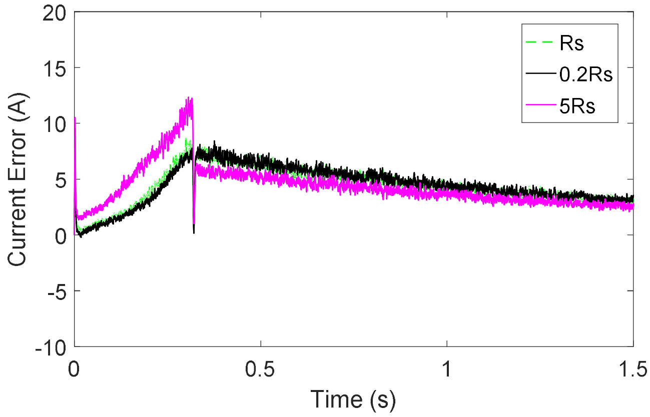

Fig. 13. Tracking error of the *q*-axis current under different stator resistance.

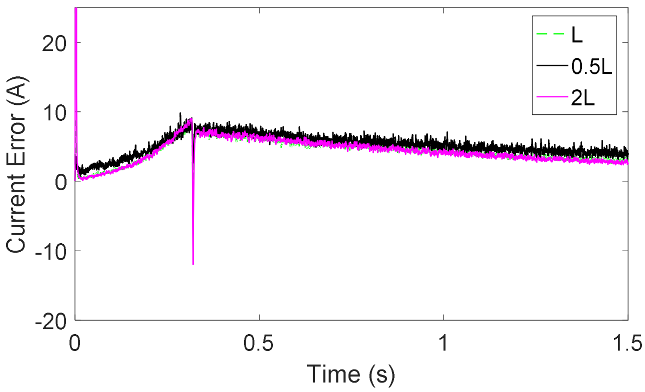

Fig. 14. Tracking error of the *q*-axis current under different stator inductance.

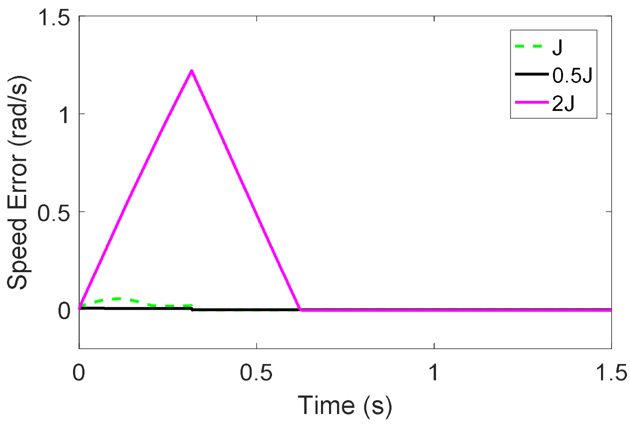

Fig. 15. Speed tracking error under different system inertia.

VI. CONCLUSIONS

In this paper, the cascaded ADRC approach was proposed to enhance the control performance of a PMSG-based tidal stream turbine. An alternative, namely a second-order ADRC was also investigated. The ADRC strategy has clearly shown key features such a lesser dependency on plant model analysis and efficient disturbance rejection capabilities. The carried out simulations and the achieved results have clearly illustrated the effectiveness of the proposed ADRC strategy under various disturbance conditions, while being compared to conventional PI and hybrid sliding mode/PI control strategies. This work has also shown that the cascaded ADRC achieves better performance than the second-order ADRC in terms of smoothed torque. Performance indices, namely ITAE and ISE, have been evaluated for three specific operating conditions. The achieved results have clearly confirmed that the proposed ADRC approach outperforms the PI and hybrid sliding mode/PI control strategies. Robustness against system parameter variations has also been investigated and verified for the cascaded ADRC approach. It has been particularly shown that the proposed ADRC approach enables slightly improving a tidal stream turbine system energy production during swell wave disturbance periods.

APPENDIX

TST System Parameters

Turbine blade radius	5.3m
Maximum C_p value	0.41
Optimal tip speed ratio for MPPT	6.3
Rated marine current speed	3.0m/s
Total system inertia	4.359×10^4 kg·m^2
System friction coefficient	0.0035
Generator nominal power	500kW
Generator nominal torque	140kNm
DC-bus rated voltage	1500V
Rotor nominal speed	34.1rpm (3.57rad/s)
Pole pair number	88
Permanent magnet flux	2.1435Wb
Generator stator resistance	0.03Ω
Generator *d-q* axis inductance	1.45mH

REFERENCES

[1] A.S. Bahaj, "Generating electricity from the oceans," *Renewable and Sustainable Energy Review*, vol. 15, no. 7, pp.3399-3416, Sept. 2011.

[2] S. Benelghali, R. Balme, K. Le Saux, M. E. H. Benbouzid, J. F. Charpentier, and F. Hauville, "A simulation model for the evaluation of the electrical power potential harnessed by a marine current turbine", *IEEE Journal of Oceanic Engineering*, vol. 32, no. 4, pp.786-797, Oct. 2007.

[3] Z. Zhou, M. E. H. Benbouzid, J. F. Charpentier, F. Scuiller, and T. Tang, "Developments in large marine current turbine technologies - A review," *Renewable and Sustainable Energy Reviews*, vol. 77, pp. 852-858, May 2017.

[4] H. Chen, T. Tang, N. Aït-Ahmed, M. E. H. Benbouzid, M. Machmoum, and M. E. Zaïm, "Attraction, challenge and current status of marine current energy," *IEEE Access*, vol. 6, pp. 12665-12685, 2018.

[5] K. Touimi, M. E .H. Benbouzid, and P. Tavner, "Tidal stream turbines: with or without a gearbox?," *Ocean Engineering*, vol. 170, pp. 74-88, December 2018.

[6] Z. Zhou, F. Scuiller, J. F. Charpentier, M. E. H. Benbouzid, and T. Tang, "Power smoothing control in a grid-connected marine current turbine system for compensating swell effect," *IEEE Transactions on Sustainable Energy*, vol. 4, no. 3, pp. 816-826, July 2013.

[7] K. J. Åström and T. Hagglund, "The future of PID control," *Control Engineering Practice*, vol. 9, no. 11, pp.1163-1175, Nov. 2001.

[8] V. Kumar, B. C. Nakra, and A. P. Mittal, "A review on classical and fuzzy PID controllers," *International Journal of Intelligent Control and Systems*, vol. 16, no. 3, pp.170-181, Sept./Dec. 2011.

[9] X. Duan, H. Deng, and H. Li, "A saturation-based tuning method for fuzzy PID controller," *IEEE Transactions on Industrial Electronics*, vol. 60, no. 11, pp. 5177-5185, Nov. 2013.

[10] A. Imura, T. Takahashi, M. Fujitsuna, T. Zanma, and M. Ishida, “Instantaneous-current control of PMSM using MPC: frequency analysis based on sinusoidal correlation,” in *Proceedings of the 2011 IEEE IECON*, pp. 3551–3556, Melbourne (Australia), Nov. 2011.

[11] M. A. M. Cheema, J. E. Fletcher, D. Xiao, and M. F. Rahman, “A linear quadratic regulator-based optimal direct thrust force control of linear permanent-magnet synchronous motor,” *IEEE Transactions on Industrial Electronics*, vol. 63, no. 5, pp. 2722–2733, May 2016.

[12] A. Levant, "Principles of 2-sliding mode design,” *Automatica*, vol. 43, no. 4, pp.576-586, April 2007.

[13] A. Levant, “Higher-order sliding modes, differentiation and output-feedback control," *International journal of Control*, vol. 76, no. 9-10, pp.924-941, 2003.

[14] Z. Gao, Y. Huang, and J. Han, “An alternative paradigm for control system design,” in *Proceedings of the 40th IEEE Conference on Decision and Control*, Orlando (USA), vol. 5, pp. 4578-4585, Dec. 2001.

[15] J. Han, “From PID to active disturbance rejection control,” *IEEE Transactions on Industrial Electronics*, vol. 56, n°3, pp. 900-906, March 2009.

[16] Y. Huang, W. Xue, Z. Gao, H. Sira-Ramirez, D. Wu and M. Sun, “Active disturbance rejection control: Methodology, practice and analysis,” in *Proceedings of the 33rd Chinese Control Conference*, Nanjing (China), pp. 1-5, July 2014.

[17] Z. Gao, “Active disturbance rejection control from an enduring idea to an emerging technology,” in *Proceedings of the 10th International Workshop on Robot Motion and Control*, pp. 269–281, Poznan (Poland), July 2015.

[18] S. Li, J. Yang, W. Chen, and X. Chen, “Generalized extended state observer based control for systems with mismatched uncertainties,” *IEEE Transactions on Industrial Electronics*, vol. 59, no. 12, pp. 4792-4802, Dec. 2012.

[19] G. Wang, R. Liu, N. Zhao, D. Ding, and D. Xu, “Enhanced linear ADRC strategy for HF pulse voltage signal injection-based sensorless IPMSM drives,” *IEEE Transactions on Power Electronics*, vol. 34, no. 1, pp. 514-525, Jan. 2019.

[20] B. Ahi and M. Haeri, "Linear active disturbance rejection control from the practical aspects," in *IEEE/ASME Transactions on Mechatronics*, vol. 23, no. 6, pp. 2909-2919, Dec. 2018.

[21] J. Yang, W. Chen, S. Li, L. Guo, and Y. Yan, "Disturbance/uncertainty estimation and attenuation techniques in PMSM drives - a survey," in *IEEE Transactions on Industrial Electronics*, vol. 64, no. 4, pp. 3273-3285, April 2017.

[22] Y. Zuo, X. Zhu, L. Quan, C. Zhang, Y. Du, and Z. Xiang, “Active disturbance rejection controller for speed control of electrical drives using phase-locking loop observer,” *IEEE Transactions on Industrial Electronics*, vol. 66, no. 3, pp. 1748-1759, March 2019.

[23] B. Guo, S. Bacha, and M. Alamir, "A review on ADRC based PMSM control designs," in *Proceedings of the 2017 IEEE IECON*, Beijing (China), pp. 1747-1753, Oct. 2017.

[24] Z. Zhou, S. Ben Elghali, M. E. H. Benbouzid, Y. Amirat, E. Elbouchikhi, and G. Feld, “Control strategies for tidal stream turbine systems – A Comparative Study of ADRC, PI, and high-order sliding mode controls,” in *Proceedings of the 2019 IEEE IECON*, Lisbon (Portugal), pp. 6981-6986, Oct. 2019.

[25] T. Ane and L. Loron, “Easy and efficient tuning of PI controllers for electrical drives,” in *Proceedings of the 2006 IEEE IECON*, Paris (France), pp. 5131-5136, Nov. 2006.

[26] Z. Zhou, “Modeling and power control of a marine current turbine system with energy storage devices,” *PhD thesis*, University of Brest (France), 2014.

[27] S. Benelghali, M. E. H. Benbouzid, J. F. Charpentier, T. Ahmed-Ali, and I. Munteanu, “Experimental validation of a marine current turbine simulator: application to a permanent magnet synchronous generator-based system second-order sliding mode control,” *IEEE Transactions on Industrial Electronics*, vol. 58, n°1, pp. 118-126, Jan. 2011.

[28] D. Liang, J. Li, and R. Qu, “Sensorless control of permanent magnet synchronous machine based on second-order sliding-mode observer with online resistance estimation,” *IEEE Transactions on Industry Applications*, vol. 53, n°4, pp. 3672-3682, July-Aug. 2017.

[29] D. H. Phan and S. Huang, “Super-twisting sliding mode control design for cascaded control system of PMSG wind turbine,” *Journal of Power Electronics*, Vol. 15, No. 5, pp. 1358-1366, Sept. 2015.

[30] L. Fridman and A. Levant, “Higher order sliding modes,” *Sliding Mode Control in Engineering*, Chapter 3, pp.1-52, Marcel Dekker, New York, 2002.

[31] W.S. Levine, “The control handbook," Section III, pp.169-173, CRC Press LLC, Florida, 1996.

[32] A. E. A. Awouda and R. B. Mamat, "Refine PID tuning rule using ITAE criteria," in *Proceedings of the 2010 IEEE ICCAE*, Singapore, pp. 171-176. Feb. 2010.

[33] P. Dahiya, P. Mukhija, A.R. Saxena, and Y. Arya, "Comparative performance investigation of optimal controller for AGC of electric power generating systems," *Automatika*, vol. 57, n°4, pp. 902-921, Dec. 2017.